This is a peer-reviewed, author's accepted manuscript of the following conference output:
da Graça Marto, S., Vasile, M., Diaz Riofrio, S., Ilioudis, C., & Clemente, C. (2022).
Survey of manoeuvre detection methods and their application to multi-static radar.
Paper presented at AMOS 2022, Hawaii, United States.

Survey of Manoeuvre Detection Methods and their Application to Multi-Static Radar

Simão da Graça Marto
Massimiliano Vasile
University of Strathclyde, Mechanical and Aerospace Engineering

Sebastian Diaz Riofrio
Christos Ilioudis
Carmine Clemente
University of Strathclyde, Electronic and Electrical Engineering

ABSTRACT

In this paper we study the benefits of using multi-static radar for manoeuvre detection in satellites. We present the conditions in which a multi-static radar is advantageous for this purpose, and show concrete results. Moreover, multiple manoeuvre detection methods from the literature are applied to this problem, and their accuracy is compared. These include optimal control based methods, and statistical methods.

1. INTRODUCTION

Since their inception, ground based space situational awareness (SSA) systems, also known as Space Surveillance and Tracking (SST), primarily have utilised radar sensors due to their ability to operate in very long ranges and under various atmospheric conditions while also providing very accurate range measurements. Initially used for early missile warning, modern SST radars are designed to monitor targets in Low Earth Orbit (LEO) up to deep space. Having very high power transmissions, in order to improve their efficiency, radar can also operate in tandem with a nearby radio telescope, forming what is known as a bistatic configuration. In this configuration, the reflected signal is received not only by the primary emitter station, but also by distant RF telescopes.

A prime example of such bistatic system is the Tracking and Imaging Radar (TIRA) located at Fraunhofer Institute for High Frequency Physics and Radar Techniques (FHR), Germany and the Effelsberg radio telescope which when paired can improve the minimum detectable target size from 2cm at 1000 km down to 1cm due to the higher sensitivity of Effelsberg. While being technically bistatic, it acts more as a quasi-monostatic radar due to the very high target altitudes. The experienced bistatic angles, β_{BS}, are generally small and the perceived radar cross section (RCS) of the target will be very similar to that of a monostatic radar. Recently, the use of long baseline bistatic radar systems for SST has been investigated within the NATO SET-293 RTG [1]. The difference with existing bistatic systems is that the RF telescopes are remotely located from the radar allowing larger bistatic angles and essentially viewing the target from different aspect angles. Specifically, capturing the target reflection in different bistatic angles can result in a higher RCS than the monostatic depending on its shape. In addition, the radar system could integrate multiple receiving signals, i.e from multiple transmitters or using multiple receivers, resulting in a higher signal to noise ratio (SNR). Moreover, combining location and velocity estimates of a target from distributed sensors can significantly improve the parameter estimation accuracy.

While preliminary analysis on captures of GEO satellites has shown that spaceborne targets can be detected in these bistatic configurations, covered research lacks from a more extensive investigation of the bespoke processing framework and performance analysis aimed at fully unlocking the benefits of such a system.

The use of tracking data from radar systems allows the reconstruction of the motion of space objects beyond the simple orbit determination. If one assumes that the object in view has a behaviour dictated by an unknown part of the

[1] https://www.sto.nato.int/Lists/test1/activitydetails.aspx?ID=16824

dynamics, it is possible to use modern machine learning techniques to reconstruct the missing part of the dynamics and recognise patterns or intentions. This process is called behaviour analysis.

In this work we assess the benefits and trade-offs of multiple behaviour analysis methods proposed in the literature, which we apply to this use-case of spacecraft being observed by bistatic or multistatic radar. We then investigate to what extent the increased data quality coming from bistatic radar observations improves the accuracy of the results of the behaviour analysis process when compared to the monostatic case. The optimal control based analyses proposed by Serra et al [9], and statistical methods such as [8] are among those tested, as well as some methods proposed by us. In general, they provide a metric that measures the likelihood that a manoeuvre was performed, and/or a mathematical description of this manoeuvre.

We consider in particular two possible scenarios: repositioning to modify its ground track, and an orbit re-positioning to shadow another satellite. For the latter, we consider the specific case of the Kosmos 2542 and 2543 satellites, which, flying in formation, approached the American KH-11 satellite in January 2020.

To summarize, we expect to obtain concrete information on the benefits of using a bistatic setup compared to a monostatic one for the purposes of behavioural analysis when applied to realistic scenarios, and investigate the quality of each method for detecting manoeuvres.

2. MANOEUVRE DETECTION

The process of manoeuvre detection consists in determining, based on observations of the state at multiple different times, if there was a manoeuvre in between. Knowledge of the state at one instant in time along with the dynamics allows predicting the state for all time, apart from deviations that can be due to manoeuvres but also sensor error and imperfect knowledge of the dynamics (often modelled as process noise). For this reason, a state observation never exactly corresponds to the expected value. To determine whether this mismatch is due to a manoeuvre or only the other two factors is the task of manoeuvre detection. All of the methods considered here produce a metric which is higher the more likely it is that a manoeuvre occurred. This is then used to obtain Receiver Operator Characteristic (ROC) curves in Section 5.

This Section describes the manoeuvre detection methods used. We will be considering cases where we have two state observations.

2.1 Optimal control based

One can safely assume that any trajectory performed by a spacecraft will be minimizing fuel consumption, as that is a critical resource for any mission. Therefore, a sensible approach is to solve the optimal control problem linking the observed states, and use as metric G,

$$\begin{aligned} G(\mathbf{x}_0, \mathbf{x}_f) = \min_u & \int_{t_0}^{t_f} \|u(t)\| \mathrm{d}t \\ s.t.\ & \mathbf{x}(t_0) = \mathbf{x}_0 \\ & \mathbf{x}(t_f) = \mathbf{x}_f \ , \end{aligned} \tag{1}$$

where $u(t)$ is the acceleration over time, and $\mathbf{x}$ is the state as the Cartesian position and velocity. The following subsections contain some examples of such methods from the literature.

2.2 Sequence of Impulses

A common simplification is to describe the manoeuvre as a sequence of impulses $\Delta v^{(i)}$, optimizing the sum of their magnitudes $G_{\Delta v} = \sum_i \Delta v^{(i)}$. We optimize this using Matlab's implementation of the interior point algorithm [1], having as control parameters the Cartesian components of each $\Delta \mathbf{v}^{(i)}$ as well as the Δt_i between consecutive manoeuvres, with $i = 1, \ldots, 5$. The process of majorization-minimization [10] is also used to deal with the undefined gradient when $\Delta v^{(i)} = 0$.

$$\begin{aligned} G_{\Delta v}(\mathbf{x}_0, \mathbf{x}_f) = & \sum_i \|\Delta v^{(i)}\| \\ s.t.\ & \mathbf{x}(t_0) = \mathbf{x}_0 \\ & \mathbf{x}(t_f) = \mathbf{x}_f \ , \end{aligned} \tag{2}$$

2.3 Continuous thrust

Alternatively, a manoeuvre can be approximated as being composed of thrust arcs with constant thrust pointing in a constant direction in the radial-trasverse-normal frame. The tool FABLE [3] efficiently produces propellant cost estimations for these types of trajectories. The references [3, 2, 6] fully describe the transcription and the algorithm used. A difference in our case is that we do not consider a departure from an hyperbolic orbit around the Earth, so the parameters describing the hyperbolic excess velocity are not used. The cost function $G_{\text{FABLE}}(\mathbf{x}_0, \mathbf{x}_f)$ is the propellant mass consumption given by FABLE.

2.4 Smooth Cost Function

In the work by Serra et al. [9], instead of minimizing G, they minimize the easier to work with G_2 given as

$$\begin{aligned} G_2(\mathbf{x}_0, \mathbf{x}_f) = \min_u \int_{t_0}^{t_f} \|u(t)\|^2 \mathrm{d}t \\ s.t.\ \mathbf{x}(t_0) = \mathbf{x}_0 \\ \mathbf{x}(t_f) = \mathbf{x}_f\ , \end{aligned} \tag{3}$$

which can be minimized using an indirect method. Even though this quantity does not correspond to the exact delta-v, the following inequality can be used to estimate it,

$$G \leq \sqrt{(t_f - t_0) G_2}\ . \tag{4}$$

A disadvantage is that the resulting control law will not be realistic, so while this method is useful for manoeuvre detection and quantification, it is not as useful for manoeuvre reconstruction.

Since in [9], the authors consider a case where only angle measurements are available, they replace the constraint on the final position in Eq. (3) by

$$\mathbf{x}(t_f) \in \Omega\ , \tag{5}$$

where Ω is the "Admissible Region", defined as the set of states that could produce the measurements observed. Because in our work we do have both range and angle measurements, affected by error, we define the Ω as confidence sets around the measurements $\mathbf{y}$, where the expected observation vector for a given state $\mathbf{x}$ is given by the observation function $h(\mathbf{x})$. Therefore, Ω is defined using the Mahalanobis distance:

$$\Omega(y) = \left\{ \mathbf{x} : (y - h(\mathbf{x}))^T R^{-1} (y - h(\mathbf{x})) < F^{(-1)}_{\chi^2_k}(p) \right\}\ , \tag{6}$$

where R is the covariance matrix of the observations, $F^{(-1)}_{\chi^2_k}$ is the inverse of the cumulative distribution function (CDF) of the chi-squared χ^2_k distribution, k is the number of individual observations in y, and p was chosen to be 0.9, such that there is a 90% likelihood of the observations lying inside the confidence interval thus defined. In this work, we define both the initial state and final state as being in a set Ω, as opposed to Serra et al. [9] who only uses an admissible region in the final state. We then obtain

$$\begin{aligned} \overline{G}_2(\mathbf{x}_0, \mathbf{x}_f) = \min_u \int_{t_0}^{t_f} \|u(t)\|^2 \mathrm{d}t \\ s.t.\ \mathbf{x}(t_0) \in \Omega(\mathbf{y}_0) \\ \mathbf{x}(t_f) \in \Omega(\mathbf{y}_f)\ . \end{aligned} \tag{7}$$

The metric $\overline{G}_2$ allows explicitly accounting for the uncertainty in the measurements, which will be shown in Section 5 to improve the manoeuvre detection accuracy.

2.5 Null hypothesis testing

Our current problem of manoeuvre detection can be viewed as one of null hypothesis testing. The null hypothesis is that no manoeuvre took place and the deviation in the measurement is due to the uncertainty in the state estimation only. Therefore, a suitable metric is the negative log likelihood of the observations assuming the null hypothesis,

$$-\log\left(p(y_f | H_0, y_0)\right)\ , \tag{8}$$

which, if we assume the distribution of the state to be Gaussian, grows monotonically with the Mahalanobis distance

$$G_{MD} = (\overline{\mathbf{x}}_f - \hat{\mathbf{x}}_f)^T (\Sigma_p + \Sigma_y)^{-1} (\overline{\mathbf{x}}_f - \hat{\mathbf{x}}_f) \ , \tag{9}$$

where $\hat{\mathbf{x}}_f$ is the predicted final state by propagating from the observation $\mathbf{y}_0$, $\hat{\mathbf{x}}_f$ is the estimate of the final state from the observation $\mathbf{y}_f$, and Σ_p and Σ_y are the respective covariance matrices. This procedure is described in [8], where it's referred to as "reachability analysis". Reachability analysis refers to any set of metrics that are based on a distance between the observed final states and the predicted states in the absence of a manoeuvre, and in fact includes the optimal control methods, where the control cost is the aforementioned distance.

In Section 5 we show that this metric produces good results, and for a test case without uncertainty in the observation of $\mathbf{x}_0$, this metric was by far the best, producing perfect results. The addition of uncertainty in $\mathbf{x}_0$ presumably leads to a departure from the Gaussian assumption due to the effect of state propagation, which could be why the metric is no longer as good for those test cases.

Even when this metric is producing perfect results, this does not mean that the other methods are useless. This method, unlike other methods, does not produce a reconstruction of the manoeuvre, whereas for instance $G_{\Delta v}$ and G_{FABLE} do.

We propose also an additional approach, based on combining the idea of minimizing within the confidence interval, used to define the $\overline{G}_2$, with null hypothesis testing. It consists in finding:

$$\begin{aligned} \overline{G}_{\text{MD}}(\mathbf{y}_0, \mathbf{y}_f) = \min_{\mathbf{x}_0} \ & (\mathbf{y}_0 - \mathbf{h}(\mathbf{x}_0))^T R^{-1} (\mathbf{y}_0 - \mathbf{h}(\mathbf{x}_0)) + (\mathbf{y}_f - \mathbf{h}(\mathbf{x}_f))^T R^{-1} (\mathbf{y}_f - \mathbf{h}(\mathbf{x}_f)) \\ & s.t. \ \mathbf{x}_f = F(\mathbf{x}_0) \ . \end{aligned} \tag{10}$$

where $F(\mathbf{x}_f)$ is the state transition function. This method has the advantage over G_{MD} that it does not require making a Gaussian approximation to the distribution of $\mathbf{x}_f$, and doesn't require any method for propagating uncertainty. An advantage it has to $\overline{G}_2$ is that it does not require the arbitrary choice of confidence interval, which sometimes leads to no solution being found.

3. MANOEUVRE DETECTION WITH BISTATIC RADAR

In monostatic radar, an electromagnetic wave or signal is emitted in a certain direction. If the signal intercepts a target, its reflection is received in the same location where it was transmitted from. We denote the range, azimuth and elevation as observed from the transmitter station as ρ_1, α_1, β_1, and their respective rates as $\dot{\rho}_1$, $\dot{\alpha}_1$, $\dot{\beta}_1$. Furthermore, ρ_1 is the position vector from the transmitter to the target.

With bistatic radar, the receiver is located far away from the transmitter, at a distance L. In this case, the bistatic range and its rate are observed, defined as $\rho_{BS} \triangleq \rho_1 + \rho_2 - L$, with ρ_1 and ρ_2 being the distance from the transmitter to the target; and the distance from the target to the receiver, respectively. We also have the observation angles and their rates as observed from the receiver station, α_2, β_2, $\dot{\alpha}_2$ and $\dot{\beta}_2$.

One disadvantage of bistatic radar is that both stations must observe the target simultaneously. This means that the transmitter and receiver antenna beams must overlap in order to generate a composite antenna beam in which the target is visible by the bistatic system. This constraint reduces the number of observation opportunities. This can be ameliorated by the addition of multiple receivers, in a multi-static configuration. Such a configuration would also provide higher quality data when multiple receivers are in line of sight of the target simultaneously.

The accuracy of the manoeuvre detection process depends not only on the metric being used, but also on the quality of the measurements, and in particular for this discussion, on the geometry of the radar transmitter, receiver, and target configuration.

Suppose we have an array of observations $\mathbf{h}(\mathbf{x})$ that allow determining the state perfectly. The variance of the state observed in this way can be approximated as

$$P = (H^T R^{-1} H)^{-1} \ , \tag{11}$$

where R is the variance of our observations, which we consider to be a diagonal matrix with the variance of each measurement. A criterion for a measurement being good at detecting a manoeuvre is the variance along the direction

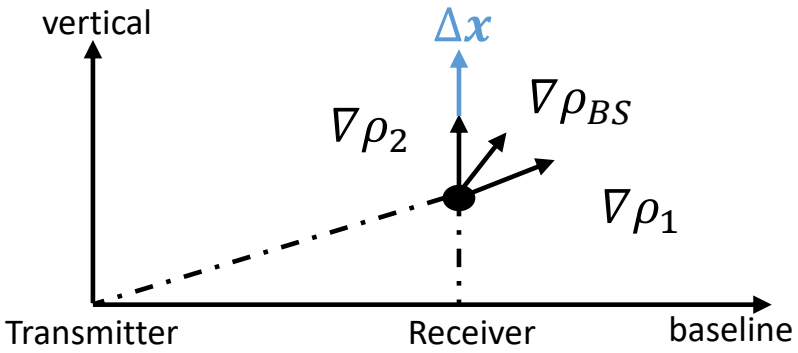

Fig. 1: Configuration of receiver and transmitter, showing the gradients of the range measurements and the direction of the state deviation.

$\Delta\mathbf{x}$ being small, which occurs when $\Delta\mathbf{x}$ is aligned with the eigenvectors with the smallest eigenvalues (variances). These will be close to the direction of the measurement with the lowest variance, coincident if H is orthogonal as is the case for monostatic observations. In our scenarios, the measurements with the lowest variance will be the range and range rate for the position and velocity respectively.

The position and velocity vectors of the target in an inertial reference frame are $\mathbf{r}$ and $\mathbf{v}$ respectively. The bistatic range is given as $\rho_{BS} = \rho_1 + \rho_2 - L$, L being the distance between the stations. The gradient of ρ_{BS} with respect to $\mathbf{r}$ is

$$\nabla_{\mathbf{r}}\rho_{BS} = \frac{\rho_1}{\rho_1} + \frac{\rho_2}{\rho_2} \,. \tag{12}$$

while the gradient $\nabla_{\mathbf{v}}\dot{\rho}$ is defined similarly.

This provides an intuition for determining when will bistatic radar provide the greatest advantage to the results. We illustrate this with a scenario, described henceforth, and with results in Section 5.1. Consider a case where the transmitter is at latitude 30ºN and the receiver, in the same meridian, is initially in the same position. Suppose a target in an equatorial orbit then performs an in-plane manoeuvre, and is observed along its orbit, such that the $\Delta\mathbf{r}$ and $\Delta\mathbf{v}$ caused by this manoeuvre are in the orbital plane, i.e. the equatorial plane. As the receiver station is brought closer to the equator, the gradient $\nabla\rho$ will have a larger projection onto the orbital plane, and thus the manoeuvre will have a larger effect on the measured range. This is illustrated for $\nabla_{\mathbf{x}}\rho = \nabla_{\mathbf{v}}\dot{\rho}$ in Fig. 1. In the latter scenario, $\nabla_{\mathbf{x}}\rho_{BS}$ can have a larger in-plane component than $\nabla_{\mathbf{x}}\rho_1$ does, which implies a lower variance for an in-plane direction. So we should expect that in these conditions, the bistatic radar measurements on their own will lead to better manoeuvre detection capabilities than monostatic, and indeed in Section 5.1 this is shown to be the case.

On the other hand, for a bistatic system, if the baseline is small, the gradient of the bistatic range measurement $\nabla\rho_{BS}$ will have similar direction to the gradient of the monostatic range $\nabla\rho_1$, and as such, will contribute mostly to lowering the variance in the direction of $\nabla\rho_1$. When the baseline is higher, $\nabla\rho_{BS}$ becomes more different to $\nabla\rho_1$, leading to lower variances along directions perpendicular to $\nabla\rho_1$. Therefore, we can expect an increase in baseline to improve manoeuvre detection results, in the general case where Δx does not align exactly with $\nabla\rho_1$.

As an illustration, if θ is the angle between $\nabla\rho_1$ and ρ_{BS}, and these observations have standard deviations of σ and 2σ (because ρ_{BS} is a sum of ranges) respectively, then the eigenvalues of P will be $\sigma^2/(1-cos(\theta))$ and $\sigma^2/(1+cos(\theta))$. Clearly, when $\theta = 0$, when the transmitter and second receiver are in the same location, one of the eigenvectors goes to infinity, as we have no information along that direction. From there, as $cos(\theta)$ increases, the eigenvalues, which again represent variances along orthogonal directions, the largest eigenvalue decreases significantly.

It can be shown[2] that if $\rho_1 \approx \rho_2 \approx \rho$, $cos(\theta) \approx \sqrt{1 - L^2/(4\rho^2)}$, which shows how an increase in baseline L leads to an improvement of the state estimation.

[2]by applying the law of cosines, followed by the half angle formula

4. QUALITY OF A METRIC

Given that we are considering a binary classifier, an ideal tool to assess a manoeuvre detection metric, is a receiver operator characteristic (ROC) curve [4]. To quantify the quality of a metric with a single value, we have the area under the ROC curve (AUC). Let G_m be the random variable for the value of a metric when a manoeuvre occurs, and G_0 when it does not. The AUC equals $P(G_m > G_0)$ [4].

To approximate the AUC for analytical purposes, we assume that the metric in consideration can be approximated as a quadratic:

$$G(\delta\mathbf{x}_0, \delta\mathbf{x}_f) \approx \frac{1}{2}\begin{bmatrix}\delta\mathbf{x}_0\\ \delta\mathbf{x}_f\end{bmatrix}^T A \begin{bmatrix}\delta\mathbf{x}_0\\ \delta\mathbf{x}_f\end{bmatrix}, \tag{13}$$

where A is the hessian matrix of G, and $\delta\mathbf{x}_0$ and $\delta\mathbf{x}_f$ are the deviation between the observed state and a pair of reference states consistent with a no manoeuvre scenario. We will now write the vector of observed states as

$$\delta\mathbf{x} = \begin{bmatrix}\delta\mathbf{x}_0\\ \delta\mathbf{x}_f\end{bmatrix} \tag{14}$$

Further, we assume that $\delta\mathbf{x}_0$ and $\delta\mathbf{x}_f$ are observed with noise that follows a Gaussian distribution with covariance matrix R and that zero mean. From these assumptions, both G_0 and G_m follow generalized chi-squared distributions, with known mean and variance [7].

To make the analysis easier, consider the following change of coordinates:

$$f_\Delta(\delta\mathbf{x}) = \begin{bmatrix}\delta\mathbf{x}_0\\ \delta\mathbf{x}_f - F(\delta\mathbf{x}_0)\end{bmatrix} \approx \Phi\delta\mathbf{x}, \tag{15}$$

where $\Delta\mathbf{x} = \delta\mathbf{x}_f - F(\delta\mathbf{x}_0)$ represents the deviation in the final state that is due to the manoeuvre, and

$$\Phi = \begin{bmatrix}I & \mathbf{0}\\ -\phi & I\end{bmatrix}, \tag{16}$$

where ϕ is the state transition matrix [11].

The hessian matrix can now be transformed into these coordinates

$$\hat{A} = \begin{bmatrix}I & \mathbf{0}\\ \phi & I\end{bmatrix}^T A \begin{bmatrix}I & \mathbf{0}\\ \phi & I\end{bmatrix} \tag{17}$$

By taking the bottom six rows and rightmost six columns of matrix $\hat{A}$, we get $\hat{A}_\Delta$, the component of the Hessian that depends on $\Delta\mathbf{x}$, leading to the following approximation of G:

$$G(\Delta\mathbf{x}) \approx \Delta\mathbf{x}^T \hat{A}_\Delta \Delta\mathbf{x}, \tag{18}$$

By making a Gaussian approximation to $G_m - G_0$, results that the AUC grows monotonically with the mean of this difference divided by its standard deviation:

$$q\{G\} = \Delta\mathbf{x}^T \frac{\hat{A}_\Delta}{\sqrt{\mathrm{tr}\,(APAP) + \delta\mathbf{x}^T APA\delta\mathbf{x}}}\Delta\mathbf{x}. \tag{19}$$

This shows that the quality of a metric depends on the particular manoeuvre being applied and when is it observed (through $\delta\mathbf{x}_f$), on the observation uncertainty (through P), and on the metric itself (through A).

In simple terms, a metric is better the more it is influenced by deviations in the estimated state caused by manoeuvres than those caused by noise. The G_{MD} metric, by weighing deviations according to their noise, achieves the second part, as the first would require knowing the manoeuvre a-priori. However, if we find the $\delta\mathbf{x}_f$ that minimizes $q\{G_{MD}\} -$

$q\{G_2\}$, one might find a $\delta\mathbf{x}_f$ that describes a manoeuvre for which G_2 has better AUC than G_{MD}. To make the optimization simpler, we can assume that $\delta\mathbf{x}_f$ is small compared to P, so that

$$q\{G\} \approx \tilde{q}\{G\} = \frac{\Delta\mathbf{x}^T \hat{A} \Delta\mathbf{x}}{\sqrt{\mathrm{tr}\,(APAP)}} = \delta\mathbf{x}_f^T A_q\{G\}\delta\mathbf{x}_f \ . \tag{20}$$

If we wish to see for which values of $\delta\mathbf{x}_f$ is $\tilde{q}\{G_{MD}\} - \tilde{q}\{G_2\}$ negative, corresponding to when we expect G_2 to be better than G_{MD}, we can look at the eigenvectors associated to the negative eigenvalues of $A_q\{G_{MD}\} - A_q\{G_2\}$. Section 5.3 has results pertaining to this.

5. RESULTS

For these tests, we assume that the observations are affected by Gaussian noise. The standard deviations for the angle measurements are given, similarly to [9], by assuming the values of α, β and ρ are observed with $n = 3$ independent observations, separated by an interval of time of $\Delta t = 20s$. We assume these observations are affected by independent Gaussian noise with standard deviations $\hat{\sigma}_\alpha = \hat{\sigma}_\beta = 1$ arcminute and $\hat{\sigma}_\rho = 100$ m. This information is turned into a tracklet $\left(\alpha, \beta, \rho, \dot{\alpha}, \dot{\beta}, \dot{\rho}\right)$ by performing a least squares fit to the data. From this process the standard deviations on the rates are also obtained. For the bistatic range, we have $\sigma_{\rho_{BS}} = 2\sigma_\rho$ and $\sigma_{\dot{\rho}_{BS}} = 2\sigma_{\dot{\rho}}$. Note that with these values, when the range is above approximately 344 km, the variance in the state estimation along the range direction will be lower than in the orthogonal directions.

An orbit without and with a manoeuvre is simulated, and observations y_0 and y_f are sampled with $N = 100$ samples for each case. These observations are simulated as having independent Gaussian noise with the standard deviations mentioned before. From these noisy observations, the states x_0 and x_f are calculated, using maximum likelihood estimates when this problem is over-determined.

5.1 Comparison of Monostatic with Bistatic Radar - Test Case 1

Following the discussion in Section 3, we present here the results where a spacecraft in equatorial orbit is observed as it crosses a meridian where two ground stations lie, the transmitter at 30º North, and the receiver on the equator. In this case, for simplicity, we assume that the initial state is known perfectly, and there is only uncertainty in the measurement of $\mathbf{x}_f$. Figure 2 shows the Receiver Operator Characteristic (ROC) curves for the G_2 metric, for monostatic, bistatic only, and the combination of the two. These curves show that using bistatic radar, in this configuration, leads to a significant improvement compared to monostatic, since the geometry of the bistatic radar in this case is such that it allows better discrimination along the direction in which the state is varying due to the manoeuvre, as explained in Section 3.

5.2 Manoeuvre Detection Methods Comparison - Test Case 2

We now present a more realistic test case. The orbit is a circular orbit with 5000 km altitude and 80 degrees inclination. The transmitter is the Millstone Hill Steerable Antenna (MISA), located at the MIT Haystack Observatory, Massachusetts, USA, and the receiver is the Westerbork Synthesis Radio Telescope (WSRT) located in Westerbork, Netherlands. The measurements are separated by approximately 7 hours, taking place approximately two orbits apart. The manoeuvre in question is an inclination change of 1 degree. This scenario is illustrated in Figure 3.

The ROC curves are shown for the monostatic observations in Fig 4 and for combined bistatic and monostatic observations in Fig 5. As expected, G_{symb} is unsuitable for this test case, since this manoeuvre is not an in-plane one. Figure 4 also shows that $G_{\Delta v}$, being closer to measuring the actual cost of a manoeuvre, leads to better accuracy than using G_2, although this advantage is less noticeable in Fig. 5. Even though G_2 and G_{FABLE} are both simulating continuous trajectories, they are optimizing different quantities, so it's interesting that their results are quite close. But in both cases, the best method for higher values of the true positive rate was $\overline{G}_2$, which can be understood as a consequence of it taking into account the uncertainty as well as applying a control distance metric. The addition of uncertainty in $\mathbf{x}_0$ could explain why the G_{MD} metric is no longer as good for these test cases, since the propagation of the state is a nonlinear process which makes the distribution of state deviation no longer Gaussian. In the definition of $\overline{G}_2$ it is only assumed that the observations have Gaussian error, which is still valid in this case.

Figures 6 and 7 show histograms with the predicted delta-v cost of the maneuver in question, compared to its real value, showing that the addition of bistatic radar leads to much closer results not just in maneuver detection, but also

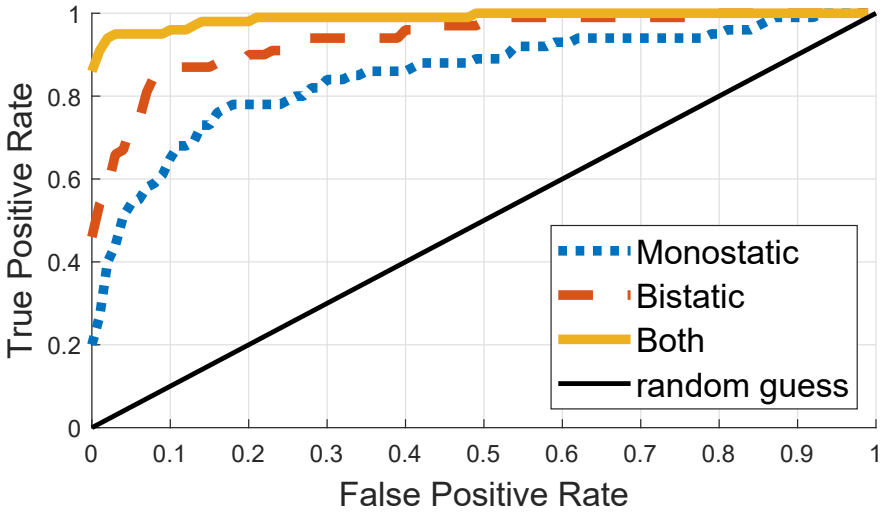

Fig. 2: ROC curve for different observation conditions

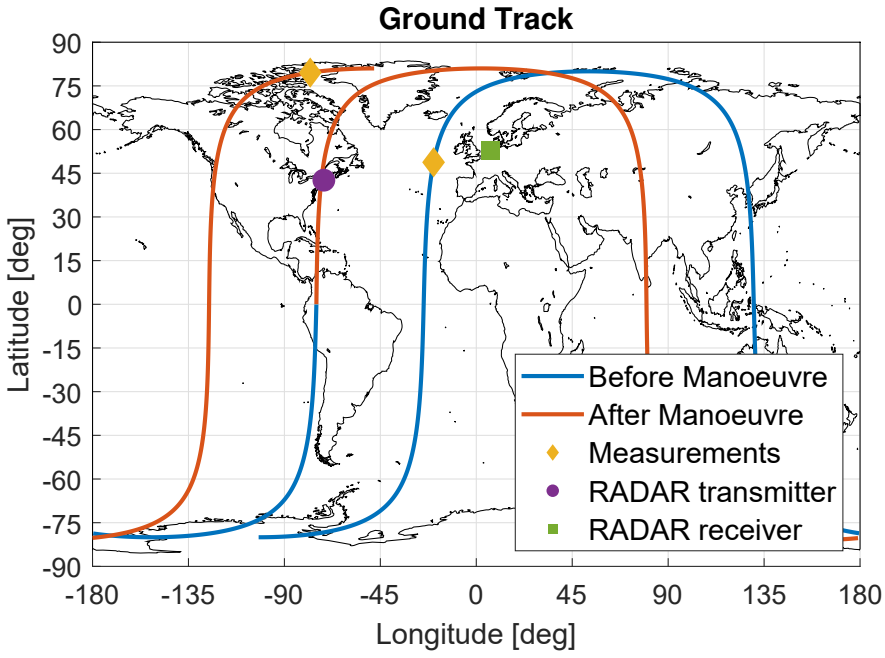

Fig. 3: Ground track for the test case 2

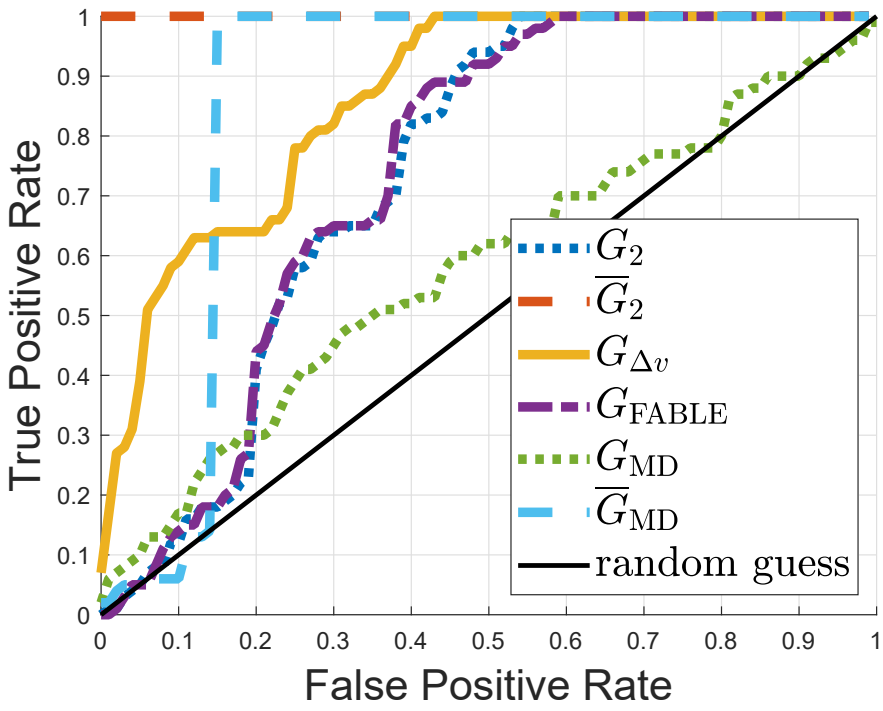

Fig. 4: ROC curves for some manoeuvre detection methods, for monostatic observation data, test case 2

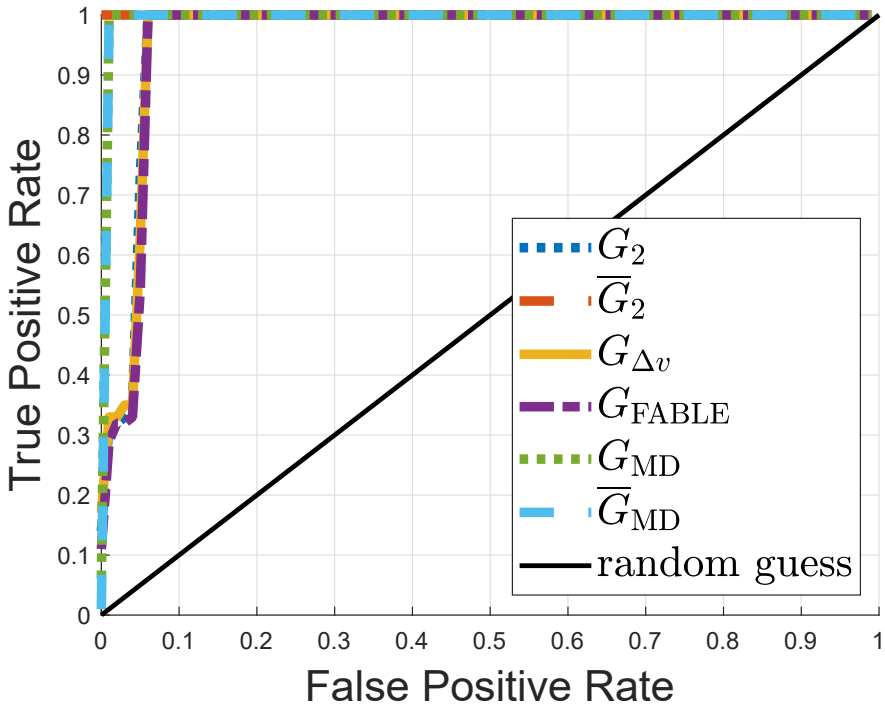

Fig. 5: ROC curves for some manoeuvre detection methods, for bistatic+monostatic observation data, test case 2

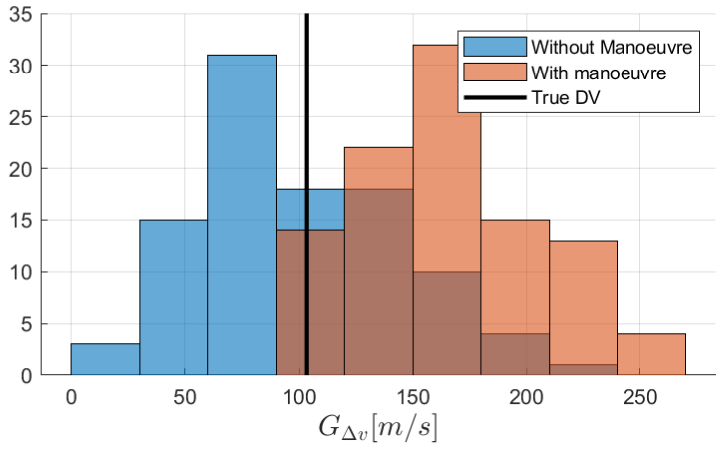

Fig. 6: Histograms of delta-v control cost as estimated using $G_{\Delta v}$, for the monostatic case.

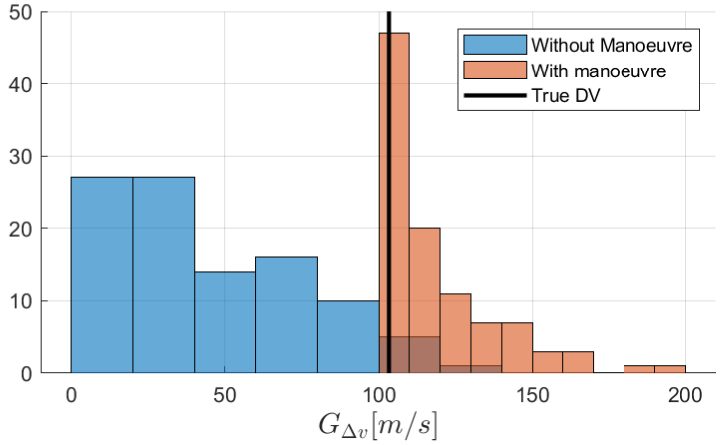

Fig. 7: Histograms of delta-v control cost as estimated using $G_{\Delta v}$, for the monostatic+bistatic case.

in its reconstruction. Numerically, the root mean squared error for the case with manoeuvre goes from 73.8m/s to 24.7 m/s by the addition of bistatic observations.

5.3 Quality of a Metric Results

We apply the theory in Section 4 to obtain, for test case 2 where typical manoeuvres produce a better result with G_{MD}, a manoeuvre for which G_2 is the better, thus demonstrating the accuracy of that theory.

For this demonstration, we use the same conditions as in test case 2, except there is only uncertainty in the second observation so as to align with the assumptions made in Section 4, and the value of the standard deviations for the measurement errors were reduced by 20, so that the small δx_f approximation can be valid. The eigenvalues of $A_q\{G_{MD}\} - A_q\{G_2\}$ are

$$\begin{bmatrix} 4.98 \times 10^9 \\ 1.36 \times 10^8 \\ 8.43 \times 10^6 \\ 1.12 \times 10^7 \\ 1.80 \times 10^3 \\ -6.16 \times 10^3 \end{bmatrix}. \tag{21}$$

The only negative eigenvalue is orders of magnitude smaller than the larger positive ones. This too supports the idea that G_{MD} is the more robust metric of the two. However, by choosing a δx_f aligned with the eigenvector corresponding

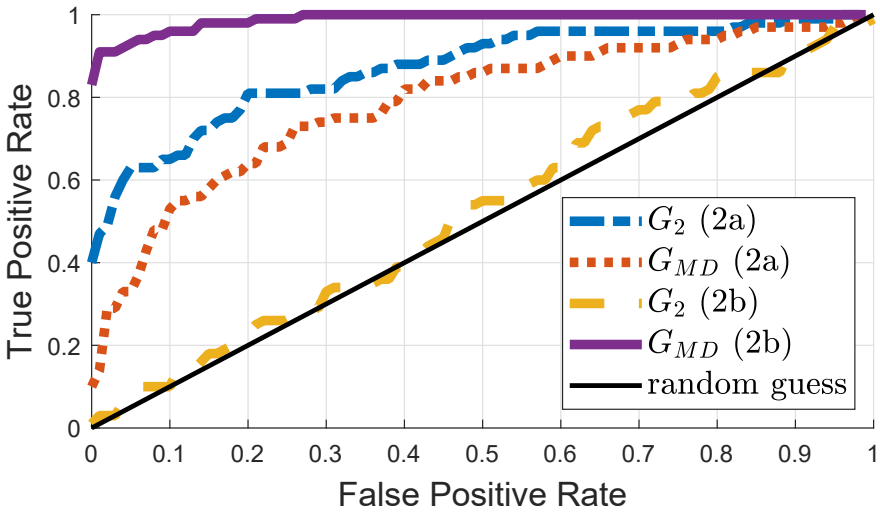

Fig. 8: ROC curves for test cases 2a and 2b.

to that negative eigenvalue, chosen such that $\sqrt{(t_f - t_0)G_2}$ is 13.9m/s, it is possible to find a manoeuvre for which G_2 is better, resulting in test case 2a, as shown in Fig. 8. That figure also includes the manoeuvre from test case 2, scaled in the same way, labeled test case 2b.

5.4 Cosmos 2542 Satellite Shadowing - Test Case 3

As realistic test case, we consider the Russian satellites Cosmos 2542 and Cosmos 2543, which in January 2020 manoeuvred so as to shadow the American satellite KH-11, also known as USA 245 [5]. By consulting the website "in-the-sky" [3], while the historical ephemerids are not available, it is possible to see graphs of the mean altitude, eccentricity, and inclination. The values around 19th January suggest an inclination change manoeuvre from around 97.9º to 97.6º, and a decrease in the apoapsis of about 58km, costing around 33m/s and 15.7m/s of delta v if they were performed by a high thrust engine.

Using this information, we model this spacecraft performing these two manoeuvres, and being observed before and after the manoeuvres, by the TIRA system located at Fraunhofer Institute.

The results are in Figure 9 for monostatic observations. Clearly, the statistical based methods G_{MD}, $\overline{G}_{\text{MD}}$ and $\overline{G}_2$ are far superior, showing perfect results. To better compare these methods, and get a better overview of the effect of having additional stations, we repeat the experiments considering two receivers, the Effelsberg 100-m Radio Telescope and the Chilbolton Observatory, see Fig. 10. The baselines of the resulting bistatic pairs are of 20km and 600km respectively. The noise on the angular measurements is also increased from one arcminute to 0.5 degrees. Figures 11 and 12 show the results for G_{MD} and $\overline{G}_{\text{MD}}$ for different combinations of receivers. The metric $\overline{G}_2$ is not included due to the very long convergence times when the noise level is this high.

Two conclusions can be reached from these results. First is that $\overline{G}_{\text{MD}}$ is superior. We note that the MC estimate of the covariance matrix used to estimate G_{MD} was obtained with 1000 sample points, which was a higher number of state propagation functions that the optimization in $\overline{G}_{\text{MD}}$ ever required for this case. Secondly, the longer baseline system improves the results significantly more than the shorter one, as expected from the discussion in Section 3.

In addition, for this test case, the eigenvalues of $q\{G_{\text{MD}}\}$ were found to always be greater than $q\{G_2\}$, indicating that there is no maneouvre, in this observation conditions, for which G_2 is better at detecting manoeuvres than G_{MD}. Furthermore, the hessian of G_{MD} was found to be identical to that of $\overline{G}_{\text{MD}}$ with relative difference in the order of 10^{-8}, suggesting that they have the same Hessian, although a theoretical proof of this is outside the scope of this work. The fact that despite this, the metrics have very different performances, shows the limitations of this method of estimating the quality of a metric, limitations which we speculate are related to the small Δx approximations taken when obtaining it.

[3] https://in-the-sky.org//spacecraft.php?id=44797

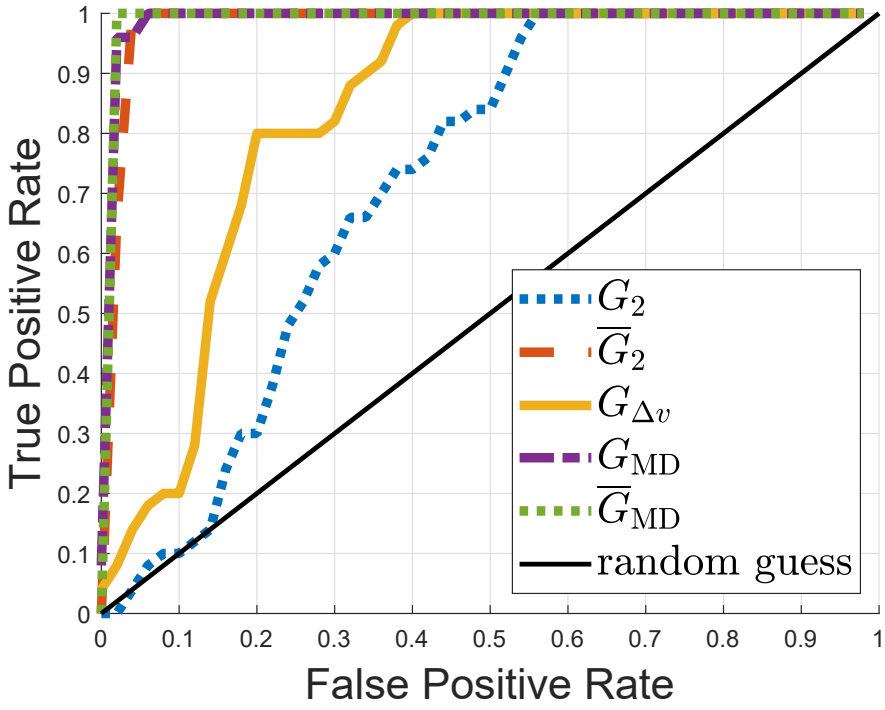

Fig. 9: ROC curves for test case 3

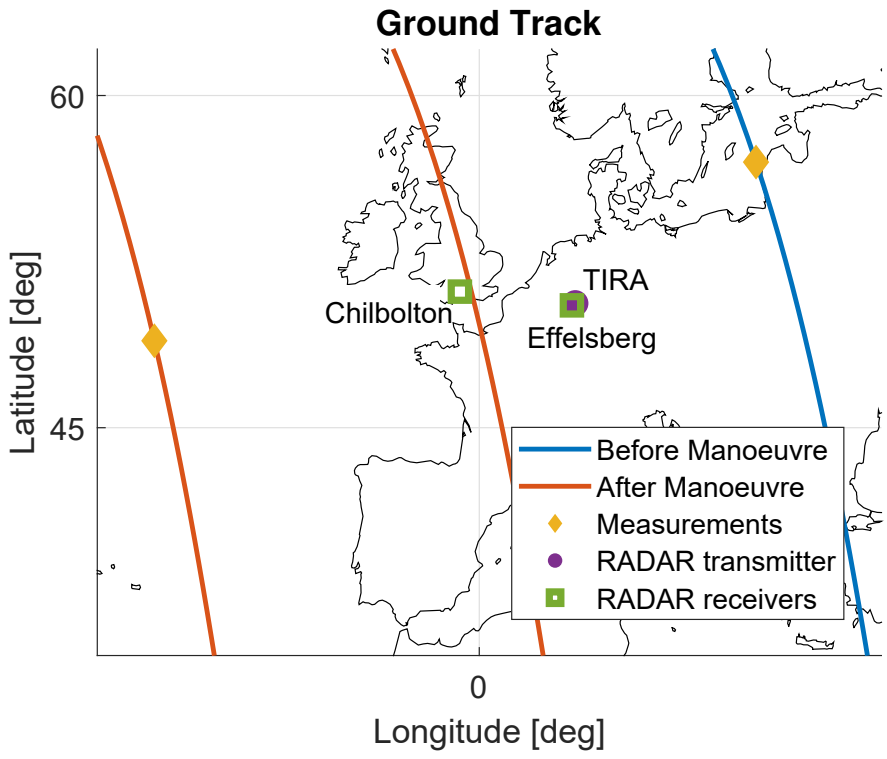

Fig. 10: Ground track and locations of transmitters and receivers for test case 3.

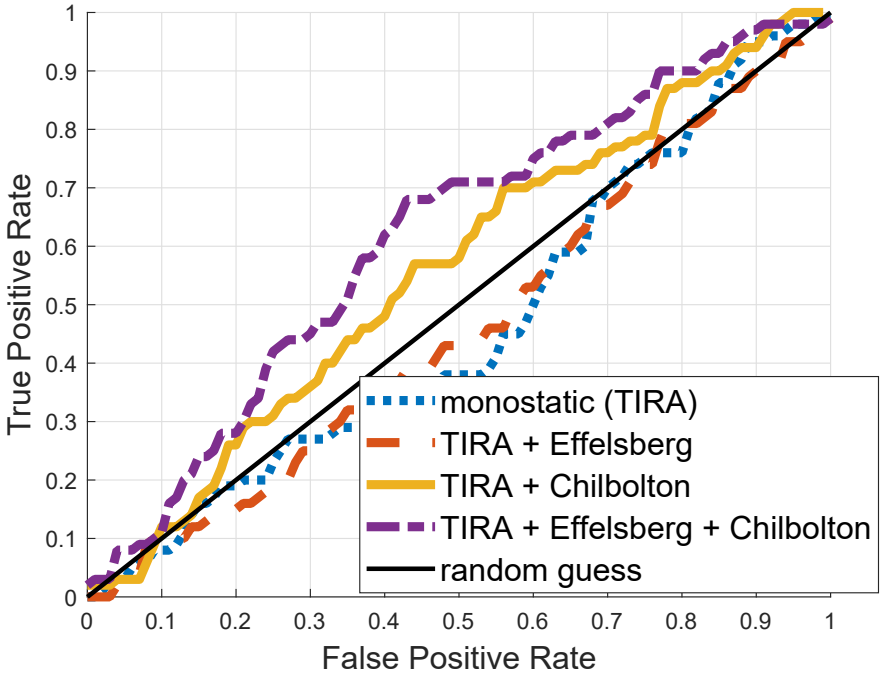

Fig. 11: ROC curves for test case 3 with angular observation noise with standard deviation of 0.5º, for metric G_{MD}

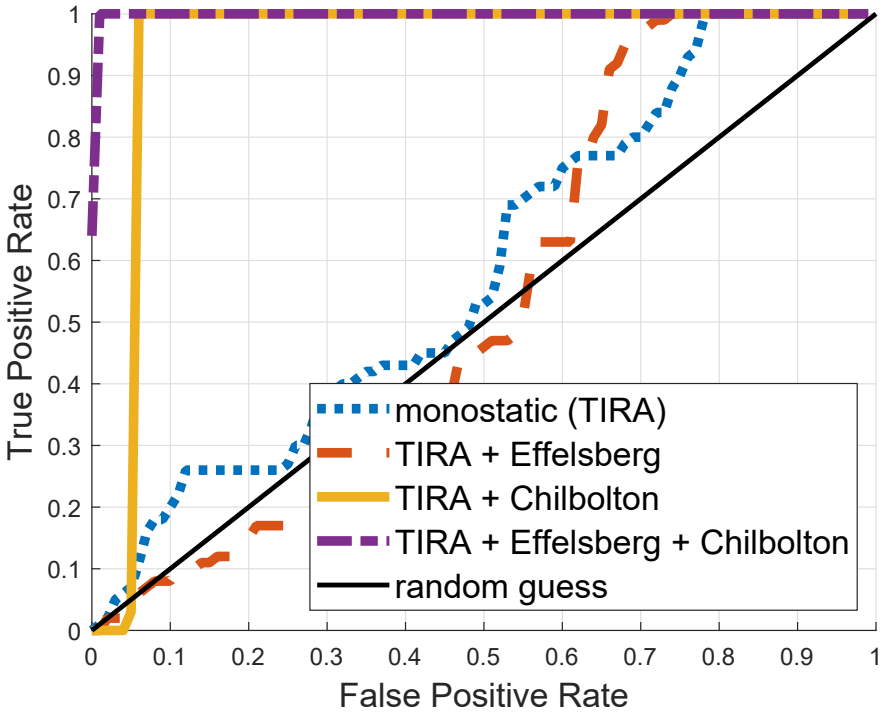

Fig. 12: ROC curves for test case 3 with angular observation noise with standard deviation of 0.5º, for metric $\overline{G}_{\mathrm{MD}}$

6. CONCLUSIONS AND FUTURE WORK

Multi-static radar, by adding extra measurement data, naturally allows improvements to the accuracy of manoeuvre detection. In this paper we showed how, for some geometries, even the data from bistatic only observations can produce better results than the monostatic radar.

We introduced a method for analytically assessing the quality of a metric for the purposes of manoeuvre detection, which depends on the response of the metric to deviations in the state, on the manoeuvre being performed, and on the measurement uncertainty. This was complemented with a literature review of manoeuvre detection methods, and their comparison based on simulated data.

In the future, we intend to investigate the use of Kalman filters, in particular those based on particle filters.

REFERENCES

[1] Richard H. Byrd, Jean Charles Gilbert, and Jorge Nocedal. A trust region method based on interior point techniques for nonlinear programming. *Mathematical Programming*, 89(1):149–185, 2000.

[2] Marilena Di Carlo, Simão da Graça Marto, and Massimiliano Vasile. Extended analytical formulae for the perturbed keplerian motion under low-thrust acceleration and orbital perturbations. *Celestial Mechanics and Dynamical Astronomy*, 133(3):1–39, March 2021.

[3] Marilena Di Carlo, Juan Manuel Romero Martin, and Massimiliano Vasile. CAMELOT: Computational-analytical multi-fidElity low-thrust optimisation toolbox. *CEAS Space Journal*, 10(1):25–36, 2018.

[4] Tom Fawcett. An introduction to ROC analysis. *Pattern Recognition Letters*, page 14, 2006.

[5] W.J. Hennigan. Exclusive: Strange russian spacecraft shadowing u.s. spy satellite, general says. *Time*, 2020.

[6] Simão da Graça Marto and Massimiliano Vasile. Many-objective robust trajectory optimisation under epistemic uncertainty and imprecision. *Acta Astronautica*, 191:99–124, 2022.

[7] A. M. Mathai and Serge B. Provost. *Quadratic forms in random variables: theory and applications*. Number v. 126 in Statistics, textbooks and monographs. M. Dekker, 1992.

[8] Jose M. Montilla, Julio C. Sanchez, Rafael Vazquez, Jorge Galan-Vioque, Javier Rey Benayas, and Jan Siminski. Manoeuvre detection in low earth orbit with radar data, 2022.

[9] Romain Serra, Carlos Yanez, and Carolin Frueh. Tracklet-to-orbit association for maneuvering space objects using optimal control theory. *Acta Astronautica*, 181, 2021.

[10] M. A. T. Figueiredo, J. B. Dias, J. P. Oliveira, and R. D. Nowak. On total variation denoising: A new majorization-minimization algorithm and an experimental comparisonwith wavalet denoising. In *2006 International Conference on Image Processing*, pages 2633–2636. IEEE, 2006.

[11] Byron D. Tapley, Bob E. Schutz, and George H. Born. *Statistical orbit determination*. Elsevier Academic Press, 2004.